

Americo Fernandez<sup>1</sup> and J. Carlos Santamarina<sup>2</sup>

## Design Criteria for Geotomographic Field Studies

**ABSTRACT:** The tomographic inversion of boundary measurements permits determining the spatial distribution of a material property within a soil mass. The most common geotomographic setup for wave-based measurements (mechanical or electromagnetic) consists of two arrays of transducers, one with sources and the other with receivers. The separation between the arrays and the number of sources and receivers have to be determined for every new field condition in order to satisfy resolution requirements in view of physical processes and mathematical constraints. The adequate design of a geotomographic study maximizes the amount of information gathered in the field, renders the maximum possible resolution within the physical constraints associated with field conditions and the available instruments, and prevents unnecessary measurement duplication.

**KEYWORDS:** tomography, nondestructive testing, geophysics, cross-hole, seismic, imaging, in situ testing, inversion, least squares, small strain

The spatial variability of soil parameters has a critical effect on all aspects of soil response, including deformation, failure propagation, liquefaction triggering and evolution, and contaminant migration. The presence of anomalies (natural or man-made) is important as well. Tomographic imaging consists of gathering data at the boundary of a body and using this information to infer the spatial variability of a property or the characteristics of inclusions within the body. The goal of this paper is to systematically analyze physical and mathematical criteria to optimize the design of geotomographic field studies.

Tomography has already played a critical role in medical diagnosis, with tools such as CAT scan, MRI, PET scan, and ultrasound imaging (1979 Nobel Prize to Cormack and Hounsfield). Physical, mathematical, and economical limitations have often hindered its development in the geosciences. Some of these issues are addressed in this study.

The first decision in the design of a geotomographic study is the type of measurement to be conducted. For example, mechanical waves provide information about the elastic properties of the medium, in particular the small-strain stiffness (which depends on the effective confinement, saturation, and soil type). On the other hand, electromagnetic waves assess the resistivity and permittivity of the soil (these parameters relate to grain size, ionic concentration, and water content). It is important to note that both types of waves provide complementary information (details and examples in Santamarina et al. 2001).

Once the type of energy flux is selected, a series of conditions and constraints must be taken into consideration to optimize the design of field measurements in order to attain the most informative dataset with minimal measurement duplication. While the discussion herein centers on seismic travel-time tomography, all concepts apply or can be readily adapted to tomographic studies with electromagnetic waves. The presentation starts with a brief review of

tomographic inversion methods in view of mathematical issues that affect experimental design. Then, physical concepts are addressed.

### Tomographic Inversion—Brief Review

The most convenient tomographic installation for near-surface geotechnical imaging is based on the cross-hole configuration, whereby the wavefront generated by a source that is excited in one borehole (“flashlight”) is simultaneously detected at the multiple receivers installed in the other borehole (“projection screen”). In the simplest case of a fairly homogeneous medium, the resulting straight ray paths are drawn in Fig. 1a.

The unknown region between boreholes is discretized into “ $n$ ” pixels, in order to produce a tomographic image of the spatial distribution of wave velocity (Fig. 1b). Given  $m$  rays, the matrix of travel length  $[L]_{m \times n}$  is formed by computing ray paths with a ray tracer algorithm and determining the length traveled by each ray inside each pixel. The travel time  $t_i$  along the  $i$ th ray is related to the travel length  $L_{i,k}$  traveled by the  $i$ th ray in each  $k$ th pixel through the velocity  $V_k$  or slowness  $S_k = 1/V_k$  of the wave across the  $k$ th pixel:

$$t_i = \sum_k L_{i,k} S_k \quad (1)$$

For all rays, Eq 1 is written in matrix form,  $[t] = [L] \cdot [S]$ , where  $[t]_{m \times 1}$  is a vector formed with all the measured travel times,  $[L]_{m \times n}$  is the matrix of travel lengths assumed from geometry or computed with a ray tracer, and  $[S]_{n \times 1}$  is a vector that contains the unknown slowness values for all pixels. Then, the inverse problem is reduced to determining  $[S] = [L]^{inv} \cdot [t]$  where  $[L]^{inv}$  is a “generalized” inverse of the matrix of travel lengths. Different algebraic techniques can be used to obtain the generalized inverse of the  $[L]$  matrix. Two methods are briefly described next (for details see Tarantola 1987; Menke 1989; Santamarina and Fratta 1998).

### Singular Value Decomposition

The matrix  $[L]$  can be decomposed into three matrices:  $[L] = [U] \cdot [\Lambda] \cdot [V]^T$  where  $[U]$  is the matrix formed by the eigenvectors of  $[L] \cdot [L]^T$ ,  $[\Lambda]$  is the matrix formed by the square root of the eigenvalues of  $[L] \cdot [L]^T$ , and  $[V]$  is the matrix formed by eigen-

Received February 14, 2002; accepted for publication November 5, 2002; published November 17, 2003.

<sup>1</sup> Senior Geotechnical Engineer, GEOCONSULT Inc., P.O. Box 362040, San Juan, PR 00969.

<sup>2</sup> Professor, Department of Civil and Environmental Engineering, Georgia Institute of Technology, Atlanta, GA 30332.

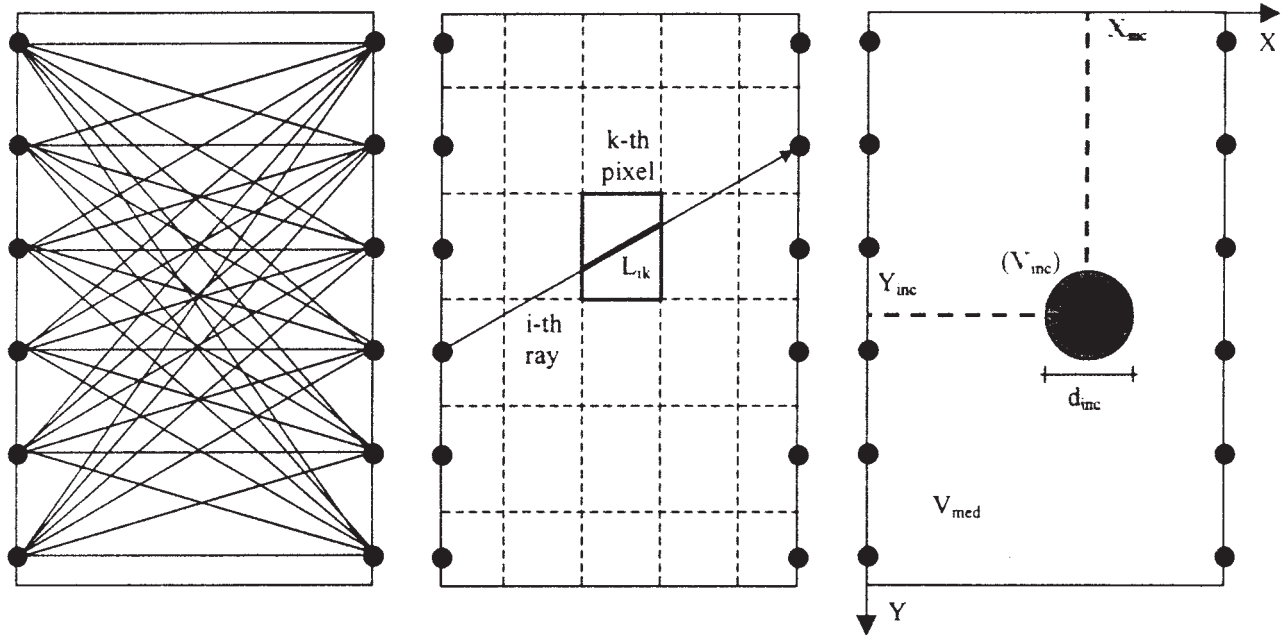


FIG. 1—Tomographic data gathering and representation: (a) ray path in cross-hole tomographic study; (b) pixel based representation; (c) medium characteristics in parametric form.

vectors of  $[L]^T \cdot [L]$ . Then, the generalized inverse is (Golub and Van Loan 1989):

$$[L]^{inv} = [V] \cdot [\Lambda]^{-1} \cdot [U]^T \quad (2)$$

In mix-determined problems, the analyst must choose the number of significant singular values “ $p$ ” that are used to obtain the generalized inverse:

$$[L]^{inv} = [V^{<p>}] \cdot [\Lambda^{<p>}]^{-1} \cdot [U^{<p>}]^T \quad (3)$$

#### Modified Least Squares

Ill-conditioning in mix-determined problems can be prevented by adding the identity matrix  $[I]$  weighted by a coefficient  $\eta$ , within the framework of least squares solutions:

$$[L]^{inv} = ([L]^T \cdot [L] + \eta^2 \cdot [I])[L]^T \quad (4)$$

This is the damped-least-squares solution. Various similar solutions are available.

#### Parameter Selection

The selection of the most appropriate value for “ $p$ ” in singular value decomposition or  $\eta$  in damped-least-squares is not trivial. In general, the higher the value of “ $p$ ” or the lower the value of  $\eta$ , the better the match between measured and predicted travel times, yet the higher the magnification of errors onto the tomographic image. The effect of noise is further addressed later in this study.

#### Inversion Related Issues

The design of a tomographic study must be intimately related to the inversion methodology and resolution expectations.

#### Number of Unknowns

Higher resolution implies smaller pixel size. As a general guiding rule, the vertical pixel size is the same as the vertical separation

between transducers within a borehole,  $\Delta z$ . For square pixels, the number of pixels in cross-hole tomography becomes:

$$\# \text{Pixels} = \text{integer} \left( \frac{H}{\Delta z} + 0.5 \right) \cdot \text{integer} \left( \frac{L_b}{\Delta z} + 0.5 \right) \quad (5)$$

where  $H$  is the depth of the tomographic image, and  $L_b$  is the separation between boreholes. The number of pixels is the number of unknowns (if there is only one unknown value per pixel, such as in isotropic media). Thus, the smaller the pixel size, the higher the number of unknowns and the more ill-conditioned the problem becomes.

#### Number of Measurements

The maximum number of possible measurements is equal to the number of sources times the number of receivers. In cross-hole tomography, with a transducer separation  $\Delta z$  in each borehole,

$$\# \text{Measurements} = [\text{integer} (H/\Delta z + 0.5)]^2 \quad (6a)$$

For example, consider a cross-hole tomographic configuration with a borehole depth  $H = 10$  m, borehole separation  $L_b = 7$  m, and transducer separation  $\Delta z = 1$  m. Then, the  $\# \text{Pixels} = 70$ , the  $\# \text{Measurements} = 100$ , and the problem appears to be “over-determined.” Geometry and the restricted radiation pattern of the transducers reduce the number of possible measurements. In this case, the asymptotic value of Eq 6a becomes:

$$\# \text{Measurements} = [\text{integer} (H/\Delta z + 0.5)] \cdot q \quad (6b)$$

where  $q$  is the number of receivers “reachable” from a given source. The lower the value of  $q$ , the more ill-conditioned the problem becomes.

#### Spatial Coverage

The simplest assessment of the spatial distribution of information is the distance traversed by the various rays in each pixel. This is the sum of all entries in the corresponding column in  $L$

(albeit, two parallel rays across a pixel do not contribute separate, “independent” information). As readily seen from Fig. 1a, there is very limited information for pixels near the top and bottom of the cross-hole setup. Therefore, even if the number of measurements exceeds the number of unknowns, the cross-hole tomographic problem based on first-arrival travel times is inherently mixed-determined.

### Non-Pixel-Based Solutions

The relatively limited amount of information available in first-arrival travel-time cross-hole tomography restricts the possible number of pixels. Hence, pixel size is often large and the resolution is low. An alternative approach is to represent the medium by some global characteristics. For example, the case shown in Fig. 1c can be captured with five unknowns: the velocity of the host medium  $V_{\text{med}}$ , the velocity and the size of the inclusion  $V_{\text{inc}}$  and  $d_{\text{inc}}$ , and its location in space  $X_{\text{inc}}$  and  $Y_{\text{inc}}$ . The rest of the discussion in this study applies whether a pixel-based or a parameter-based representation is used.

### Physical Restrictions To Resolution

The wavelength,  $\lambda$ , defines the maximum resolution that can be achieved in the field. In general, anomalies smaller than one wavelength cannot be detected by cross-hole tomography. Therefore, the test resolution is restricted by the characteristic frequency  $f$  generated by the source and by the nominal velocity of the medium  $V_{\text{med}}$ , so that  $\lambda = V_{\text{med}}/f$ .

### Diffraction Around Low-Velocity Anomalies

The detection of low-velocity anomalies (e.g., cavities) is restricted by diffraction healing: when the transmitted wave diffracts around the anomaly, the front tends to “heal” after the anomaly, effectively hiding its presence about two wavelengths behind (Fig. 2). For example, an anomaly of diameter  $D = \lambda$  at the center of the region can be detected if the separation between boreholes is smaller than  $\sim 5\lambda$ . Note that high-velocity anomalies may effectively appear as low-velocity anomalies when they have a very high impedance contrast with the medium and virtually no energy is transmitted across the anomaly, that is, when  $V_{\text{inc}} \rho_{\text{inc}} \gg V_{\text{med}} \rho_{\text{med}}$ , where  $V$  and  $\rho$  are the velocity and mass density corresponding to the medium “med” and the inclusion “inc.”

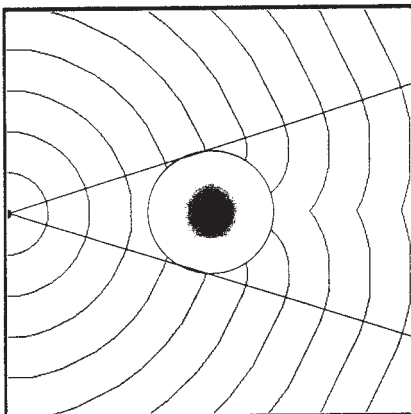


FIG. 2—The effect of diffraction healing for low velocity inclusions (computed with a Huygen’s based simulation).

### Detectability—Change in Travel Time Due to the Presence of an Inclusion

The presence of an inclusion alters the travel time along a ray that passes through it. Consider a source-to-receiver distance  $L$  in a medium of velocity  $V_{\text{med}}$  and an inclusion of diameter  $d_{\text{inc}}$  and velocity  $V_{\text{inc}}$ . Then, the relative change in travel time due to the presence of the inclusion is:

$$\frac{\delta t}{t_{wo}} = \frac{t_w - t_{wo}}{t_{wo}} = \frac{\frac{L_b - d_{\text{inc}}}{V_{\text{med}}} + \frac{d_{\text{inc}}}{V_{\text{inc}}}}{\frac{L_b}{V_{\text{med}}}} - 1 = \frac{d_{\text{inc}}}{L_b} \left( \frac{V_{\text{med}}}{V_{\text{inc}}} - 1 \right) \quad (7)$$

where  $t_w$  and  $t_{wo}$  are the travel times with and without the inclusion, respectively. The value of  $\delta t$  must exceed the precision in travel time measurements  $\varepsilon_t$ . Figure 3 shows contour lines of normalized change in travel time. The range of anomaly characteristics, in terms of  $V_{\text{inc}}/V_{\text{med}}$  and  $d_{\text{inc}}/L_b$ , where detection is not possible is highlighted for precision  $\varepsilon_t = 1$  and 3 %.

### Transducer Related Issues

The design of a tomographic experiment must also take into consideration the inherent characteristics of transducers. Salient properties are discussed next.

### Source Energy and Frequency Content

The selection of the source is intimately related to the frequency range in the transmitted wave in order to attain the required resolution. In general, the larger the source and the higher the energy it delivers, the lower the frequency content. This trend is captured in Fig. 4.

### Receivers

Displacement, velocity, or acceleration transducers can be used. While geophones are almost exclusively employed in classical seismic testing (10–100 Hz), either geophones or accelerometers are used in high-resolution tomographic applications (500 Hz to a few thousand Hz). Geophones are selected so that their resonant frequency is five to ten times lower than the operating frequency. The opposite applies to accelerometers.

### Radiation Pattern—Aperture

The radiation pattern of an installed transducer (source or receiver) depends on the geometry of the transducer, its coupling to the medium, and the direction of the excitation. Boundary conditions, such as a borehole casing and the soil-casing relative impedance, affect the radiation pattern and the effective size of the source (Gibson and Peng 1994). For example, a 0.2-m-long borehole source may effectively appear as a few metres long source if the casing is much stiffer than the surrounding soil. A typical radiation pattern for a vertically excited point in an infinite medium is shown in Fig. 5a. The amplitude of radiated  $S$ -waves (solid line in Fig. 5a) is highest between  $\pm 45^\circ$ .  $P$ -wave radiation lobes are aligned with the excitation; the compression front travels in the direction of the excitation and a rarefaction front travels in the opposite direction.

The radiation pattern limits the range of relative source-receiver locations (Refer to Eq 6b). For the case shown in Fig. 5a, the reception of  $S$ -waves will be weak at receivers located above or be-

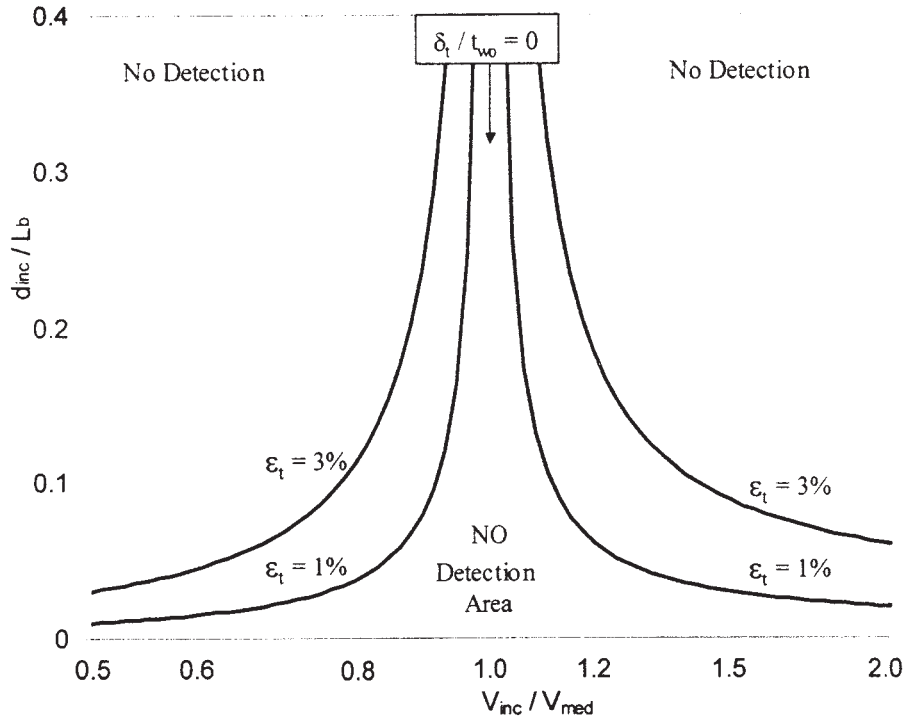


FIG. 3—Anomaly detection. Minimum size and velocity contrast for travel-time based detection (Eq 7). The NO Detection Area is bounded for two levels of travel time precision  $\epsilon_t = 1\%$  and  $3\%$ .

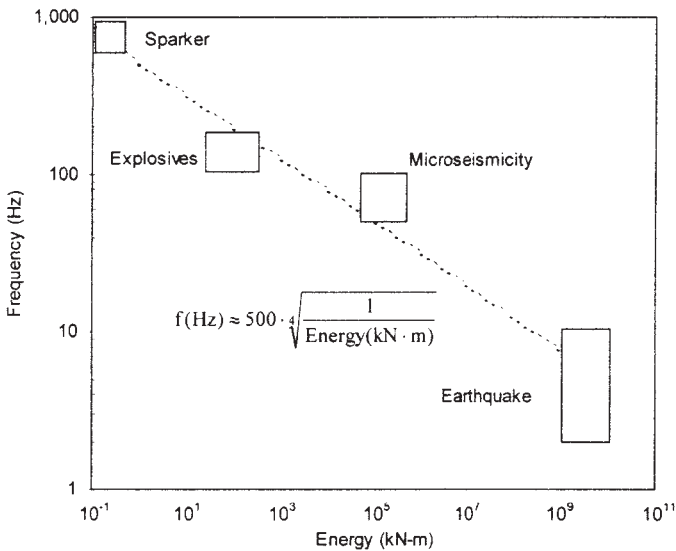


FIG. 4—Source: Trade-off between delivered energy and frequency content.

low the level of the source at an angle greater than  $\beta_{max} \approx |45^\circ|$ . Furthermore, the strong *P*-wave component at greater angles adds difficulty to the detection of *S*-wave arrivals.

The maximum illumination angularity  $\beta_{max}$  related to the transducers' radiation pattern restricts the ability to resolve the lateral extent of an inclusion, as shown in Fig. 5*b*. The distance between boreholes may be reduced to constrain the lateral extent of the anomaly in low  $\beta_{max}$  cases. However, higher sampling frequencies and higher frequency sources must be used if the inter-borehole distance  $L_b$  is reduced.

Source Generated Noise—Tube Wave

Unwanted signals that are coherently generated by the source itself cannot be readily filtered or cancelled. For example, the support of a weight drop system vibrates when the mass is released, causing an unwanted signal prior to the main excitation.

A particular case of source-generated noise is the propagation of an energy front along a fluid-filled borehole, or tube-wave. For a fluid-filled borehole (Radius  $b$ ) in a soil formation (shear modulus  $G_s$ ), the tube velocity  $V_T$  in the fluid is (density  $\rho_f$  and bulk modulus  $B_f$ —White, 1965—see also Burridge et al. 1993):

$$V_T = \left[ \rho_f \cdot \left( \frac{1}{B_f} + \frac{1}{G_s} \right) \right]^{-0.5} \quad (\text{for uncased boreholes}) \quad (8a)$$

and if the borehole is cased (casing thickness  $h$ , Young's modulus  $E_c$ ):

$$V_T = \left[ \rho_f \cdot \left( \frac{1}{B_f} + \frac{2b}{E_c \cdot h} \right) \right]^{-0.5} \quad (\text{for a thin-walled casing}) \quad (8a)$$

Propagating tube waves irradiate energy into the medium, according to the relative impedance of the fluid and the surrounding medium. In addition, when the traveling front reaches the bottom of the borehole, it emits *P*- and *S*-waves into the medium (Lee and Balch 1982). These wave fronts interfere with those radiated at the source and add difficulty to the interpretation of seismic records in soils (for a case history, see Fernandez et al. 2002).

Near Field and Far Field

The near field is the region close to the source where the propagating perturbation is not properly formed, either (1) due to the superposition of dilatational and shear waves or (2) due to the interference of wavelets generated from different regions at the

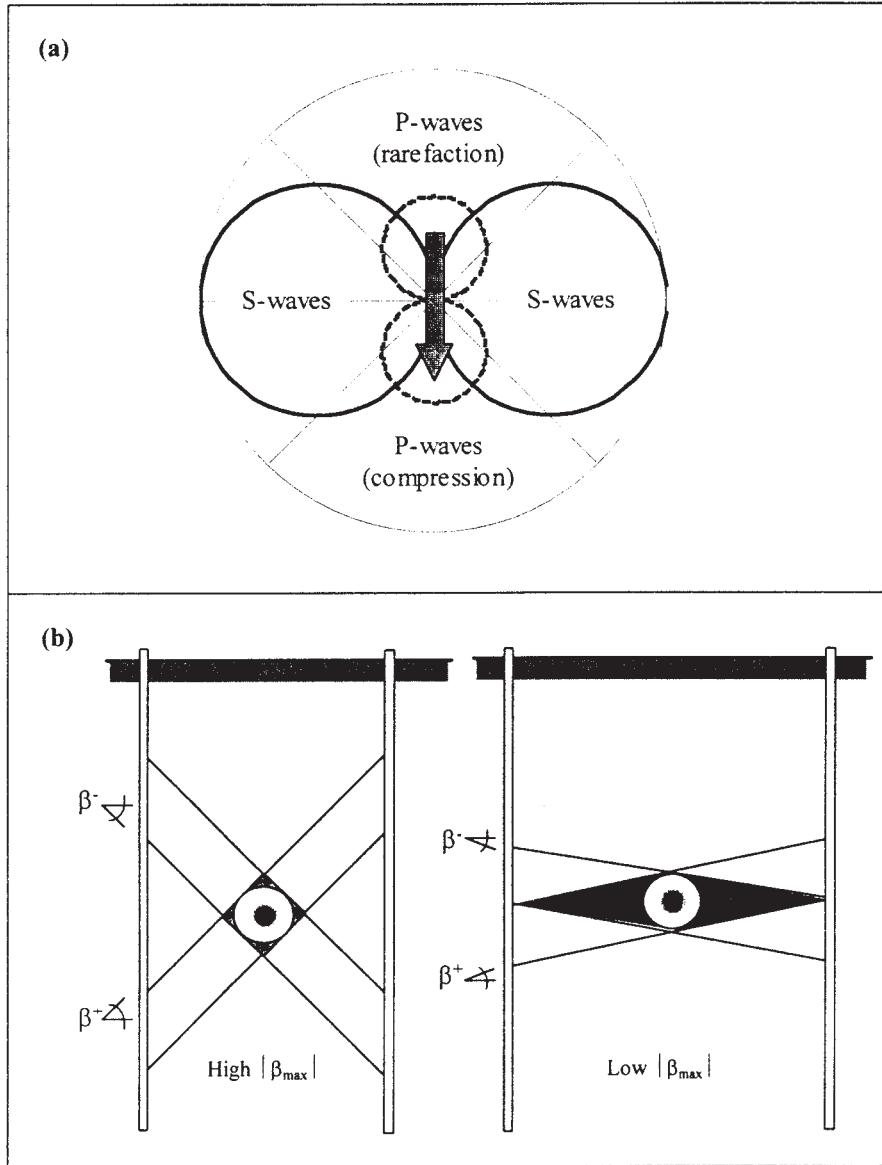


FIG. 5—Radiation patterns—sources and receivers: (a) vertically excited point in an infinite space (Poisson’s ratio  $\nu = 0.1$ —Equations in White, 1983); (b) limited illumination angle: when illumination rays are at  $\beta^+$  and  $\beta^-$ , the shaded regions cannot be illuminated (high impedance mismatch), and there is poor lateral constraining of anomalies.

source face. In the first case, a travel distance greater than two  $P$ -wave wavelengths is needed in an infinite medium to avoid the interaction between the radiated  $P$  and  $S$  waves from a point source (this applies for a period-long wavelet and  $V_p \approx 1.5V_s$ ; see White 1983). In the second case, the superposition of Huyghens wavelets emitted from the face of a circular source of radius  $R$  shows that the near field can be disregarded when the observation point is at a distance  $x$  from the source greater than about  $x > R^2/\lambda$ . At shorter distances, the spatial frequency, the amplitude, the particle motion, and the wave front are altered (Hueter and Bolt 1955; Krautkrämer and Krautkrämer 1990; Sánchez-Salinerio et al. 1986).

**Transmission Related Issues—The Medium**

Soil type, effective confinement, diagenetic effects (such as cementation), and water content determine the  $P$ - and  $S$ -wave ve-

locities ( $V_p$  and  $V_s$ ). Guidelines in Table 1 can be used to estimate the wave velocity for a given soil deposit.

The small-strain material damping  $D$  is strain-rate, frequency-dependent when viscous losses prevail in wet soils. Typical values for material damping at small strains and at frequencies relevant to high-resolution field tests (100 Hz–2 kHz) are summarized in Table 1.

*Attenuation, Dynamic Range, and Penetration Distance*

In a homogeneous medium without loss, the relationship between the amplitudes  $A_1$  and  $A_2$  at two points at distances  $r_1$  and  $r_2$  from the source is given by:

$$\frac{A_2}{A_1} = \left(\frac{r_1}{r_2}\right)^n \tag{9}$$

where the exponent  $n$  depends on the geometry of the wave front:  $n = 0$  for plane waves,  $n = 1/2$  for cylindrical waves, and  $n = 1$  for

TABLE 1—Seismic wave propagation in soils—velocity and damping.

$V_s$ [m/s]	$V_s = \psi \cdot \left( \frac{\sigma'_{mean}}{1 \cdot \text{kPa}} \right)^\beta$	Soft clays: $\beta = 0.25 - 0.35$ Dense sands: $\beta = 0.20 - 0.25$ Cemented/OC: $\beta = 0 - 0.1$ General - all soils: $\psi[\text{m/s}] = 700(0.36 - \beta)$
$V_p$ [m/s]	Saturated Soil: $V_p = V_{pf} \sqrt{\frac{\theta}{[n\alpha + (1-n)][n + (1-n)G_s]}}$ Poisson's ratio $\mu \approx 0.5$	$V_{pf} = 1500$ m/s grain/fluid stiffness $\theta \sim 20$ to 40 specific gravity $G_s = 2.7$
	Saturation < 99%: $V_p \approx 1.5 V_s$	Poisson's ratio $\mu \approx 0.1$
Damping [%]	Saturated Soft Clays Wet Sand Dry Sand	D~ 1.0 - 5.0 D~ 0.1 - 3.0 D~ 0.3 or lower

Notation:  $V_s$ : S-wave velocity.  $V_p$ : P-wave velocity.  $\sigma'_{mean}$ : mean effective stress.  $n$ : porosity. D: Damping.

Compiled from: Vucetic and Dobry (1991), Fernandez 2000, Santamarina et al. (2001).

spherical waves. Material losses cause additional attenuation and are captured in the attenuation coefficient  $\alpha$  (which is related to the damping ratio  $D$  and the wavelength  $\lambda$  as  $\alpha = 2\pi D/\lambda$ ). Then, Eq 9 becomes

$$\frac{A_2}{A_1} = e^{-\alpha(r_2-r_1)} = e^{-(2\pi D/\lambda)(r_2-r_1)} \quad (10)$$

The amplitude of the signal at the receiver  $A_2$  must be significantly larger than the noise amplitude  $N$ . Combining this observation with Eqs 9 and 10, the inter-borehole distance  $L_b$  must satisfy the following relation (presumes  $L_b \gg r_1$ ):

$$\left( \frac{r_1}{L_b} \right)^n e^{-2\pi DL_b/\lambda} \frac{A_1}{N} > \frac{A_2}{N} \quad (11)$$

A minimum value of  $A_2/N$  around  $\sim 100$  should be considered (i.e., about 40 dB). This condition can be satisfied by: (1) reducing the inter-borehole spacing  $L_b$ , (2) allowing a lower signal-to-noise ratio at the receiver  $A_2/N$  through proper filtering or signal stacking, or (3) increasing the energy at the source  $A_1$  (however, this may cause a decrease in frequency content, as shown in Fig. 4). A larger source  $r_1$  or a longer wavelength  $\lambda$  would hinder resolution.

Figure 6 shows the maximum borehole separation as a function of material damping  $D$  and wavelength  $\lambda$  for spherical propagation ( $n = 1$ ). The other parameters are selected to reflect common field situations. In particular, the equivalent size of the source  $r_1$  is assumed to be  $r_1 \approx 0.30$  m, which is appropriate for boreholes without casing. Note that while geometric spreading prevails in elastic wave propagation (Eq 11), material damping can play an important

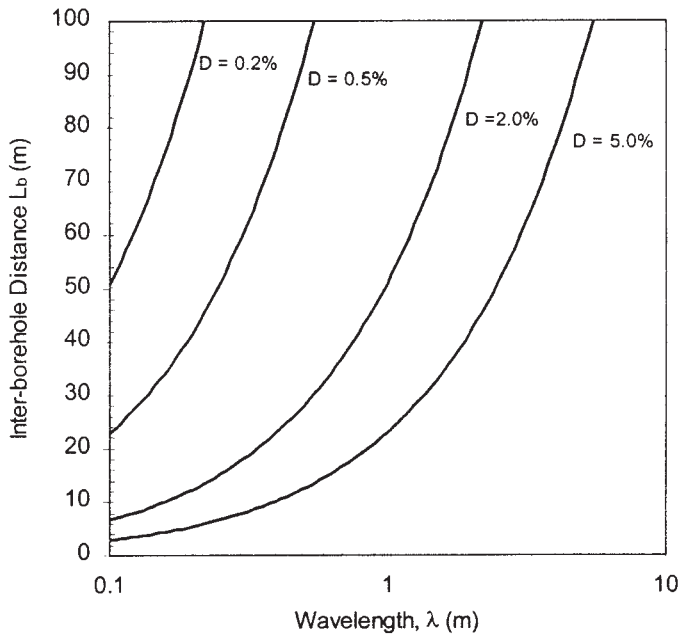


FIG. 6—Damping ratio and inter-borehole separation. Computed with Eq 11 assuming  $A_1/N = 10^7$  (140 dB),  $A_2/N = 100$  (40dB)  $n = 1$  (cylindrical front), and source size  $r_1 = 0.3$  m. The maximum inter-borehole distance is estimated from an estimate of the wavelength (propagation velocity in the soil and frequency of the source) and the soil-damping ratio.

role in the total attenuation the spherical front experiences. This effect can be critical in electromagnetic wave propagation where conduction losses are often high (e.g., moist clayey soils or when the pore fluid has high ionic concentration).

### Ray Curvature

The simplest and most robust tomographic inversion takes place when straight ray paths can be assumed between sources and receivers (i.e., linear inversion). However, the ray path is curved in heterogeneous media, including media with gradually varying stiffness, such as near-surface soil deposits (anisotropy aggravates this situation). In such conditions, ray paths tend to go deeper into the deposit, where high confining stresses provide higher velocity for the traveling wave. The error in travel time between the fast curved ray and the assumed straight ray is maximum for horizontal rays.

In order to minimize errors in travel time computation, the horizontal separation between sources and receivers  $L_b$  can be restricted so that the error associated with the straight ray assumption is in the same order of magnitude as the error in travel time measurement  $\varepsilon_t$ . Figure 7 presents the normalized error in travel time, defined as:

$$\text{Normalized Error} = \frac{(\text{Time}_{\text{straight\_ray}}) - (\text{Time}_{\text{curved\_ray}})}{(\text{Time}_{\text{curved\_ray}})} \quad (12)$$

The travel time for curved rays is computed with a close form solution for a medium with wave-velocity increasing linearly with depth  $z$  ( $V_{\text{vert}} = a + b \cdot z$ ), and with anisotropy  $c = V_{\text{vert}}/V_{\text{hor}}$  defined as the ratio between the velocity in the vertical direction  $V_{\text{vert}}$  and the velocity in the horizontal direction  $V_{\text{hor}}$  (solution in Santamarina and Fratta 1998).

Results in Fig. 7 suggest that for velocity anisotropy up to  $c = 1.2$ , the error associated with the simplified straight ray assumption is smaller than about 1 to 2 % when the depth of the source  $z_s$  is greater than 1.5 to 2 times the inter-borehole separation  $L_b$ . This limitation favors deep, closed-spaced configurations, where the near-surface velocity gradient is less important.

### Limiting Separation between Transducers (Sources or Receivers)

Redundant measurements increase time and cost, and do not necessarily improve the inverted image. To avoid redundancy, transducers in each borehole should be adequately separated. The Fresnel's ellipse for a source-receiver pair provides insight into this decision. The ellipse is drawn with foci located at the positions of the source and the receiver, with a cord length  $L_b + \lambda/2$  (Fig. 8a). The separation  $\Delta z$  between contiguous transducers within a borehole should be selected to minimize the intersection between two consecutive ellipses yet leaving no regions uncovered. On the basis of these arguments, the optimal transducer separation within a borehole is about  $\lambda/2$ .

The separation between consecutive transducers must also recognize the detectable difference in travel time between two consecutive receivers (Fig. 8b). Given the precision in travel time detection  $\varepsilon_t$ :

$$\Delta z \geq \sqrt{L_b \cdot V_{\text{med}} \cdot \varepsilon_t} \quad (13)$$

This criterion often imposes a larger transducer separation  $\Delta z$  than the Fresnel condition. Therefore significant effort must be dedicated to increasing the precision in travel time determination (i.e., reducing  $\varepsilon_t$ ) in order to enhance tomographic resolution.

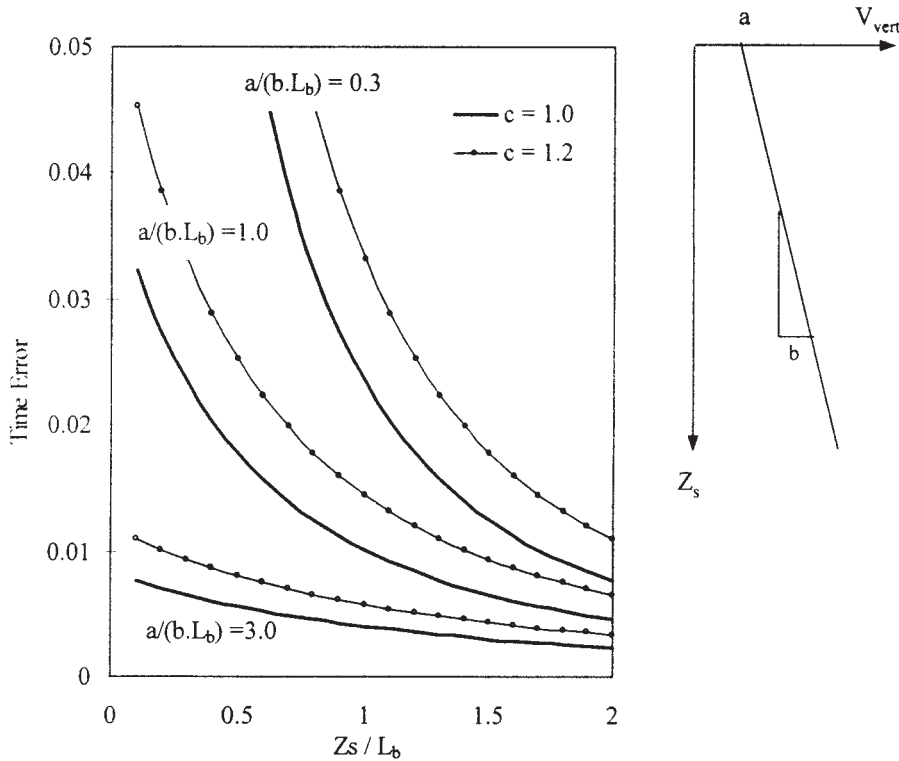


FIG. 7—Normalized error in travel time when straight rays are assumed. In this medium, the vertical velocity  $V_{\text{vert}}$  increases linearly with depth at a rate “ $b$ ,” starting with velocity  $V_{\text{vert}} = a$  at surface. The velocity anisotropy is  $c = V_{\text{vert}}/V_{\text{hor}}$ . The source is at depth  $Z_s$ . The inter-borehole separation  $L_b$  must be selected so that the model travel time error is similar to the measurement travel time error  $\varepsilon_t$ .

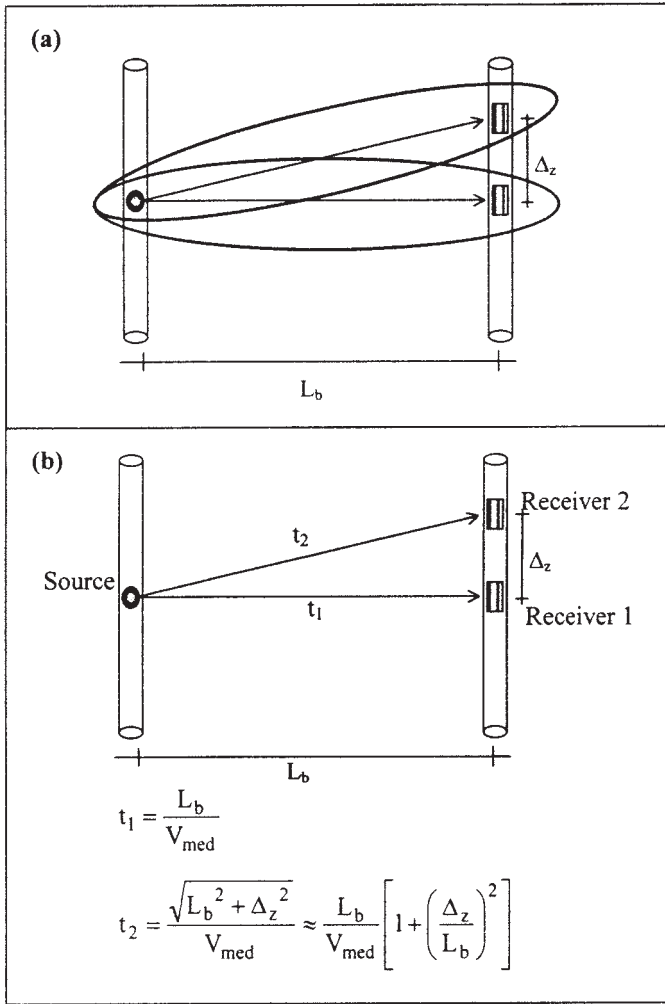


FIG. 8—Separation between transducers. Two criteria: (a) Fresnel's ellipse; (b) precision in travel time.

**Measurements and Model Errors—Noise**

Errors in the vector of measured travel times  $[t]$  and in the matrix of travel lengths  $[L]$  are magnified during the inversion process and may render a meaningless set of pixel slowness  $[S]$ . Errors in  $[L]$  are the result of the incorrect location of transducers (e.g., unknown borehole inclination) or inappropriate ray tracing (e.g., invalid straight-ray assumption). Thus, the careful implementation of test procedures and the adequate selection of ray tracing algorithms reduce errors in  $[L]$ .

On the other hand, errors in travel time  $[t]$  tend to be more insidious, more difficult to diagnose, and have a stronger detrimental effect on the results. Noise control and optimal inversion with noisy data are briefly discussed next.

*Background Noise—Control*

Data gathering for near-surface tomographic studies are often conducted at sites where various sources of noise are present (e.g., microseismicity, industry-machinery, traffic). The level of background noise defines the lowest possible amplitude of the arriving signal. If the noise has energy in the frequency range of the signal, frequency domain filtering is not adequate. Yet, if the background noise is stationary and ergodic, and if the source and trigger are re-

peatable, then signal stacking is the most robust procedure to increase the signal-to-noise ratio.

The number of signals that must be measured and stacked  $N_{meas}$  to have 95 % confidence that the peak-to-peak amplitude  $A_{p-p}$  is within 5 % of the true value can be estimated using statistical concepts:

$$N_{meas} = \left( 40 \frac{\sigma_{noise}}{A_{p-p}} \right)^2 \tag{14}$$

In this equation, the standard deviation  $\sigma_{noise}$  is determined from the entries in a time series of recorded noise (without source excitation). And, a first estimate of the value of  $A_{p-p}$  is obtained from a time series gathered while exciting the source.

*Triggering Error*

Systematic triggering errors cause a constant time-shift in all measurements. This error cannot be corrected by stacking multiple signals, and system calibration is required. In some cases, the systematic error can be detected by measuring the travel time to receivers located at different distances from the source in a homogeneous medium; then, a plot of the measured travel times versus distance readily denounces the triggering error as the time intercept at zero distance.

*Precision in Travel Time Determination #1*

The determination of travel time is a salient source of error. Near field effects, multiple propagation paths, and interference aggra-

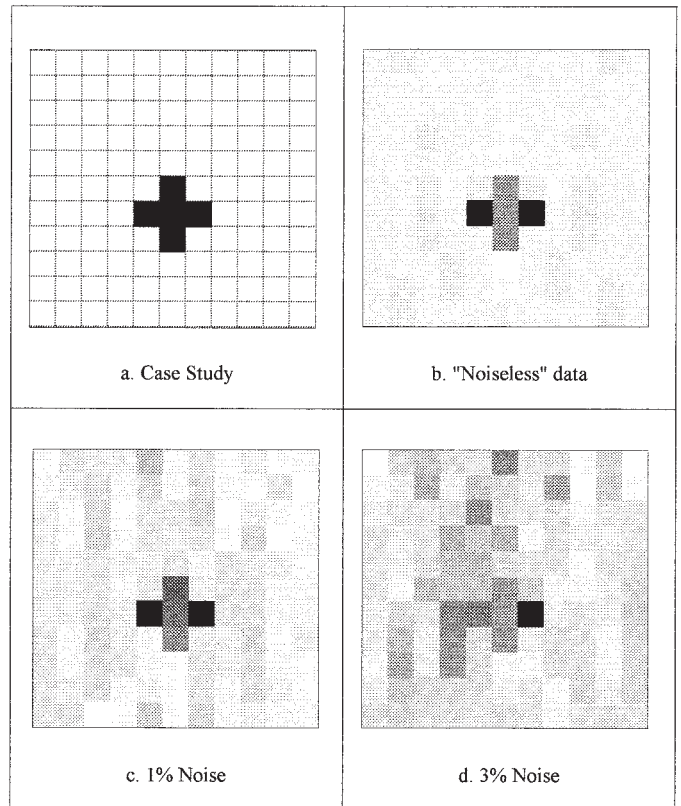


FIG. 9—Inversion procedure and noise level: (a) case under consideration; (b)–(d) tomographic images using 85% of all singular values ( $p = 103$ ).

vate this situation. Automated algorithms may be time-efficient and repeatable, but their precision depends on the validity of the assumed criteria. Signal processing tricks suffer similar fate (e.g., cross-correlation, cepstrum analysis, analytical signal).

The precision in travel time determination by picking first arrivals by hand is about a tenth of the period, that is,  $\epsilon_t \approx (10 \cdot f_{\text{signal}})^{-1}$ . If phase comparison can be applied, phase differences  $\Delta\phi$  as small as milliradians can be detected, and the precision in travel time determination is  $\epsilon_t \approx \Delta\phi \cdot (2\pi \cdot f_{\text{signal}})^{-1}$ . In all cases, precision is enhanced by operating at the highest possible frequency  $f_{\text{signal}}$  (in addition, near field effects are reduced as well).

*Error Level and Inversion Procedure*

The inversion methodology can be optimized to render the most credible tomogram for a given level of measurement or model error. This involves the selection of resolution or pixel size (thus, the number of pixels and the resulting ill-conditioning), as well as the level of damping, the amount of regularization or the number of

selected singular values. The following example highlights this observation.

Consider the case shown in Fig. 9a. The problem corresponds to a space discretized into an 11 by 11 grid with 11 sources and 11 receivers. For the purposes of this analysis, a contrasting cross-shaped anomaly is simulated (made of five pixels; medium velocity 200 m/s; anomaly velocity 1000 m/s), yet cross-hole travel times are synthetically generated using straight rays. Measurement noise is simulated by randomly adding a travel time error to each measurement. Three levels of random noise are simulated: (1) no noise, (2) up to  $\pm 1\%$ , and (3) up to  $\pm 3\%$  of the travel time  $t_i$ . The generalized inverse is computed using singular value decomposition. Figures 9b, 9c, and 9d present the tomographic images for the three levels of noise, obtained using the largest 85% of all singular values ( $p = 103$ ). The sequence of images clearly shows that the quality of tomograms degrades as the noise level increases.

Inversions are repeated for each level of noise, using different numbers of singular values  $p$  (Fig. 10a). Each computed tomogram

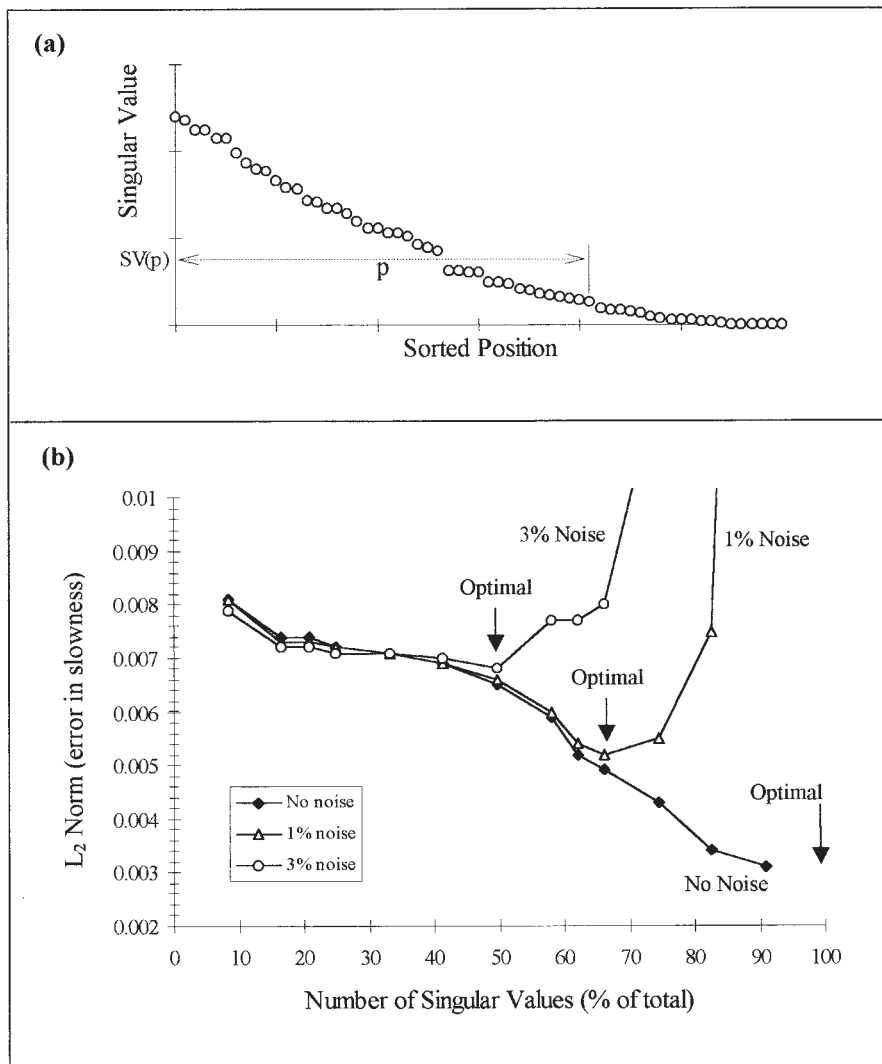


FIG. 10—The optimal number of singular values  $p$  that should be used to obtain a tomogram decreases as the noise level increases: (a) singular values sorted by magnitude—the total number of singular values is 121; (b) error between the obtained image and the original case in Fig. 9a—the optimal value of  $p$  is shown for each level of noise.

TABLE 2—Summary of design consideration—nonlinear decision process.

<b>JOB REQUIREMENTS - RELATED TO ENGINEERING NEEDS</b> Depth of Exploration [H] Length to be explored [ $L_{exp}$ ] Size of anomalies to be detected [ $d_{inc}$ ]- Resolution Nature of anomalies – Low impedance or high impedance relative to medium Type of Parameters (seismic or electromagnetic)		
<i>Needed Preliminary Information:</i> estimated site conditions such as velocity $V_{ned}$ and damping D; knowledge of the scale of heterogeneity and the degree of anisotropy is valuable.		

Design Parameter		Determined by	Affects / Relates to
Operating Frequency [f]		Resolution and penetration	Transducer selection Number of pixels Accuracy in travel time Transducer separation Size of near-field
Borehole	Depth [H]	Pre-determined (see Job Requirements)	
	Borehole Separation [ $L_b$ ]	Damping and frequency Geometric spread Dynamic range in acquisition system Uncertainty due to ray curvature Anomaly constraining $H > L_b$ Low-or-high velocity anomaly (diffraction?)	The number of tomographic images is $L_{exp}/L_b$
	Casing	Minimize impedance contrast Avoid tube waves (do not fill with water)	
Transducers	Source Type	To attain needed frequency (Also: availability)	Frequency
	Receiver Type	Compatible with selected frequency	Frequency
	Transducer separation [ $\Delta z$ ]	Fresnel ellipse Attainable precision in travel time	Frequency Resolution Number of pixels
	Aperture	Directivity pattern (predetermined for a selected transducer-installation condition)	Ray selection for given source ("rays used")
Data	Sampling rate [ $\Delta t$ ]	Aliasing: 10 times faster than the higher frequency of interest (use antialiasing filter)	Frequency
	Duration	Two-three times the travel time	Required memory
	Stacks	Noise level	Affects possible resolution
	Spatial coverage and ray pattern	Accessibility to the boundaries of the body and Spatial distribution of transducers Directivity of transducers	Source and receiver
Inversion	Problem Representation	Options: Pixel vs. parametric Available information	Resolution Robust inversion Ill-posedness
	Type of inversion	Data pre-processing and noise reduction With initial guess Including additional information	Noise level Depends on availability of information

is compared to the true image (Fig. 9a), and the sum squared error is evaluated,  $L2\text{-norm} = \sum (S_k^{true} - S_k^{inv})^2$  Figure 10b shows the results. The best image is obtained for the values of  $p$  that minimize the  $L2\text{-norm}$ . Clearly, the higher the level of noise, the lower the value of  $p$  that must be selected. Unfortunately, there are no simple a priori criteria that can be used to select  $p$  in real field situations; hence, the burden rests on the analyst.

**Recommended Procedure for Tomographic Studies**

The previous discussions are summarized in Table 2. Entries under "Job Requirement" list the main constraints and expectations. Decisions that must be made to gather the data are listed under "Test Parameters." This column also includes implications immediately relevant to the inversion methodology. Design decisions are interconnected and the design process is nonlinear. The main interrelations are listed in the last column.

**Conclusions**

Geotomography consists of inferring the spatial variability of a soil parameter from boundary measurements. Wave-based tomography, using either elastic or electromagnetic waves, can render valuable soil parameters for engineering design.

The design of a geotomographic study must take into consideration physical principles, mathematical constraints, and engineering needs. The different variables are interrelated and the design process is nonlinear.

The frequency content of the signal is the most critical parameter. It defines: resolution, penetration, and inter-borehole separation, transducer separation, extent of the near field, and the precision in travel time determination.

As pixel size  $b$  decreases, resolution increases as  $b^{-1}$ , the number of pixels (or unknown pixel values) increases as  $b^{-2}$  and the number of measurements in cross-hole tomography settings in-

creases as  $b^{-1}$ . Therefore ill conditioning and error amplification also increase.

Noise, measurement errors, and inadequate model assumptions effectively reduce the amount of information that can be extracted from the measurements and decrease the attainable resolution.

#### Acknowledgement

This study was conducted by the authors at the Georgia Institute of Technology. Funding was provided by PDVSA-Intevep and the National Science Foundation. The authors are grateful to A.R. Crumley at GeoConsult, Inc.

#### References

- Burridge, R., Kostek, S. and Kurkjian, A. L., 1993, "Tube Waves, Seismic Waves and Effective Waves," *Wave Motion*, Vol. 18, pp. 163–210.
- Fernandez, A. L., 2000, *Tomographic Imaging the State of Stress*, Ph.D. dissertation, Georgia Institute of Technology, May 2000.
- Fernandez, A., Gonzalez, M., Parra, S., Malave, G., Alvarelos, J., and Santamarina, J. C., 2002, "Tomographic Imaging the Sub-surface Beneath a Dam—Inferring the State of Stress," *Proceedings, Canadian Dam Conference*, October, Victoria.
- Gibson, R. L. and Peng, C., 1994, "Low and High Frequency Radiation from Seismic Sources in Cased Boreholes," *Geophysics*, Vol. 59, No. 11, pp. 1780–1785.
- Golub, G. H., and Van Loan, C. F., 1989, *Matrix Computations*, Johns Hopkins University Press, Baltimore.
- Hueter T. F. and Bolt R. H., 1955, *Sonics*, John Wiley and Sons, Inc. New York, New York.
- Krautkrämer, J. and Krautkrämer, H., 1990, *Ultrasonic Testing of Materials*, Springer-Verlag, Berlin, Germany.
- Lee, M. W. and Balch, A. H., 1982, "Theoretical Seismic Wave Radiation from a Fluid-Filled Borehole," *Geophysics*, Vol. 47, No. 9, pp. 1308–1314.
- Menke, W., 1989, *Geophysical Data Analysis: Discrete Inverse Theory*, International Geophysics Series, Academic Press, San Diego.
- Sánchez-Salinero, I., Roesset, J. M., and Stokoe, K. H., 1986, *Analytical Studies of Body Wave Propagation and Attenuation*, Geotechnical Engineering Report GR86-15, University of Texas at Austin, Austin.
- Santamarina, J. C. and Fratta, D., 1998, *Introduction to Discrete Signals and Inverse Problems in Civil Engineering*. ASCE Press, Virginia.
- Santamarina, J. C., Klein, K., and Fam, M., 2001, *Soils and Waves*, J. Wiley and Sons, Chichester, UK.
- Tarantola, A., 1987, *Inverse Problems Theory*, Elsevier, Amsterdam.
- Vucetic, M. and Dobry, R., 1991, "Effect of Soil Plasticity on Cyclic Response," *Journal of Geotechnical Engineering*, Vol. 117, No. 1, pp. 89–107.
- White, J. E., 1965, *Seismic Waves: Radiation, Transmission, and Attenuation*, McGraw-Hill, New York.
- White, J. E., 1983, *Underground Sound*, Elsevier, New York.